Tiny Molecular Beacons: LNA/2′-*O*-methyl RNA Chimeric Probes for Imaging Dynamic mRNA Processes in Living Cells

Irina E. Catrina,[†] Salvatore A. E. Marras,[‡] and Diana P. Bratu*[,†,§]

[†]Biological Sciences Department, Hunter College, City University of New York, New York, New York 10065, United States

[‡]Public Health Research Institute, Department of Microbiology and Molecular Genetics, University of Medicine and Dentistry of New Jersey, Newark, New Jersey 07103, United States

[§]Program in Molecular, Cellular, and Developmental Biology, and Program in Biochemistry, The Graduate Center, City University of New York, New York, New York 10016, United States

Ⓢ *Supporting Information*

ABSTRACT: New approaches for imaging dynamic processes involving RNAs in living cells are continuously being developed and optimized. The use of molecular beacons synthesized from 2′-*O*-methylribonucleotides (which are resistant to cellular nucleases) is an established approach for visualizing native mRNAs in real time. In order to spatially and temporally resolve dynamic steps involving RNA in cells, molecular beacons need to efficiently hybridize to their RNA targets. To expand the repertoire of target sites accessible to molecular beacons, we decreased the length of their probe sequences and altered their backbone by the inclusion of LNA (locked nucleic acid) nucleotides. We named these new LNA/2′-*O*-methyl RNA chimera oligonucleotides "tiny molecular beacons". We analyzed these tiny molecular beacons and found that the incorporation of just a few LNA nucleotides enables these shorter probes to stably anneal to more structured regions of the RNA than is possible with conventional molecular beacons. The ease of synthesis of tiny molecular beacons and the flexibility to couple them to a large variety of fluorophores and quenchers render them optimal for the detection of less abundant and/or highly structured RNAs. To determine their efficiency to detect endogenous mRNAs in live specimens, we designed tiny molecular beacons that were specific for *oskar* mRNA and microinjected them into living *Drosophila melanogaster* oocytes. We then imaged the live oocytes *via* spinning disk confocal microscopy. The results demonstrate that tiny molecular beacons hybridize to target mRNA at faster rates than classically designed molecular beacons and are able to access previously inaccessible target regions.
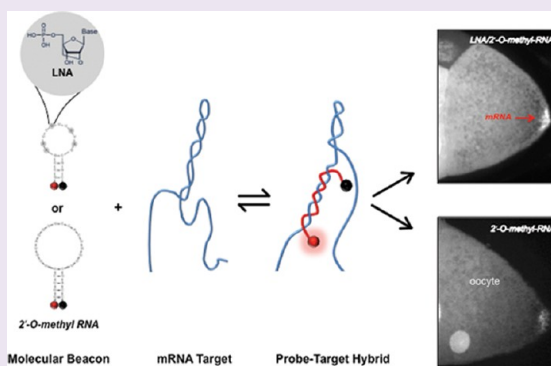
For years, only a static view of the steady-state distribution of endogenously expressed mRNAs was possible utilizing mRNA *in situ* hybridization.[1] However, in 1993 Ainger and colleagues brought the field of *in vivo* RNA imaging onto the front pages of scientific journals by injecting and imaging *in vitro*-transcribed, fluorescein-labeled myelin basic protein (MBP) mRNA in cultured mouse oligodendrocytes.[2] The fluorescent RNA formed particles that moved throughout the cell at rates similar to that of kinesin, a plus end-directed microtubule motor protein. Since then, this method has been widely used to study the transport of localized mRNAs in other cell types and in tissues of various species.[3−5] Though very valuable, this approach raised some questions, as *in vitro*-transcribed labeled mRNAs may not reflect the behavior of endogenous mRNA. When mRNA is transcribed *in vitro*, it evades the nuclear processing it may require to properly be transported and localized in the cell.[6] Therefore, the RNA-protein particles may be missing important nuclear factors that, in turn, fail to recruit other cytoplasmic factors that are required for efficient transport and localization.

Consequently, a handful of approaches have been developed to visualize endogenous RNAs in subcellular space in real time, which have enabled unprecedented insights into the dynamic properties of RNAs.[7,8] Sanjay Tyagi elegantly summarized the imaging methods to date that illuminate mRNAs using labeled oligonucleotide probes, fluorescent protein tags, and aptamers that render organic dyes fluorescent.[9] Moreover, his review explores the promises and limitations of these methods. Among them is the molecular beacons technology, which utilizes probes that fluoresce only upon hybridization to specific complementary mRNA sequences.[10] Introduced as an innovative and general approach, molecular beacons have been used in a variety of cell types, detecting mRNA at various levels of expression.[11−14] Coupled with fast three-dimensional imaging over time, molecular beacons technology enables time-resolved studies of RNA-protein interactions *in vivo* and

provides details of the dynamically orchestrated relationship between an mRNA and the various proteins involved in its transport.[15]

Molecular beacons are internally quenched hairpin-shaped oligonucleotide probes that fluoresce upon hybridization with complementary sequences within the target mRNA (Figure 1, panel a).[10] Target-bound probes fluoresce up to 100 times more intensely than unbound probes, enabling highly sensitive detection. They are designed with the aid of the *mfold* web server, an algorithm that predicts nucleic acid folding and
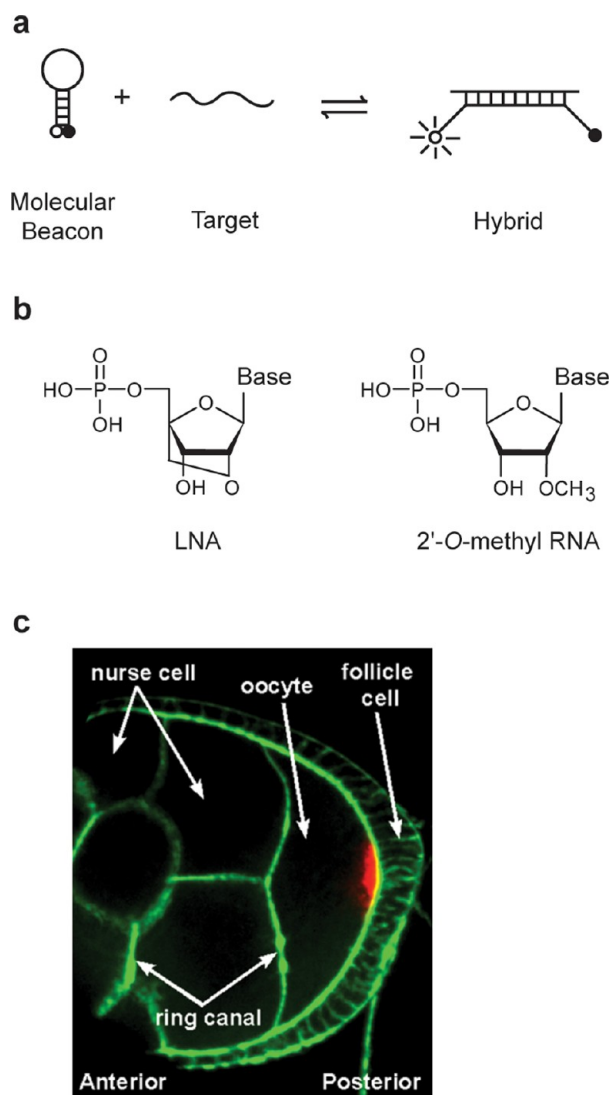
Figure 1. Principle of operation of molecular beacons. (a) Schematic representation of molecular beacon function. In the absence of a complementary nucleic acid target, molecular beacons are non-fluorescent, as the hairpin conformation keeps the fluorophore (F) in close proximity to the quencher (Q). In the presence of a target, the probe sequence in the loop anneals to the target forming a stable and rigid double helix, thereby unfolding the stem hybrid, resulting in the separation of the quencher from the fluorophore, leading to the generation of a bright fluorescence signal. (b) Molecular structure of an LNA nucleotide and a 2′-O-methylribonucleotide. (c) *oskar* mRNA localization (red) in a fixed *Drosophila melanogaster* egg chamber at mid-oogenesis, as detected with the *2′OMe-RNA 2209* molecular beacon. *oskar* mRNA is transported from the nurse cells to the oocyte through ring canals *via* a microtubule-dependent process. Actin was stained with Phalloidin-FITC (green).

hybridization based on thermodynamic considerations.[16,17] A well-designed molecular beacon forms a stable hairpin conformation under physiological conditions. The most stable predicted structure must be a hairpin, ensuring that the fluorophore and quencher are in close proximity. Molecular beacons can be synthesized from modified nucleotides (*e.g.*, 2′-O-methylribonucleotides[18] or LNA (locked nucleic acids) nucleotides[19]) to ensure greater stability of the probe and of the probe−target hybrid; these molecular beacons can be labeled with a wide variety of fluorophores, enabling detection of multiple targets simultaneously.[20]

Using non-natural backbone modifications is especially important when these probes are used for live cell imaging, in order to (i) ensure that the probe is resistant to cellular nucleases, (ii) increase the stability of the hybrid that is formed with the target RNA, and (iii) prevent the degradation of the target RNA by cellular RNase H.[21] LNA is a nucleic acid modification in which the 2′ oxygen atom and the 4′ carbon atom in the furanose ring are bridged *via* a methylene moiety (Figure 1, panel b).[22] The effect of LNA substitutions on probe-hybrid stability is approximately additive when LNA nucleotides are spaced by at least one 2′-O-methylribonucleotide.[23] On average, an internal LNA substitution for a 2′-O-methylribonucleotide increases duplex stability by −1.4 kcal/mol at 37 °C (eq 1). This corresponds to a 10-fold increase in the probe's binding constant.[23]

$$\Delta G^{\circ}_{37}(\text{chimera/RNA})$$
$$= \Delta G^{\circ}_{37}(\text{2}'\text{-}O\text{-MeRNA/RNA}) - 1.1 n_{iAL/UL}$$
$$- 1.6 n_{iGL/CL} \tag{1}$$

ΔG°_{37} (2′-O-MeRNA/RNA) is the free energy change at 37 °C for duplex formation in the absence of any LNA nucleotides, and $n_{iAL/UL}$ and $n_{iGL/CL}$ are the numbers of internal LNAs in AU and GC pairs, respectively.

Besides the makeup of the nucleic acid backbone, probe−target hybrid stability depends on the length of the molecular beacon's probe sequence and its GC sequence content. Molecular beacons work best when they are designed to form an 18−25 nucleotide-long duplex with >30% GC content. Unfortunately, these parameters limit target selection to RNA stretches that are extensively single-stranded or are only slightly structured, as predicted by RNA folding programs.[24]

Here, we describe the development of an extension of molecular beacons technology that allows access to RNA target regions that are otherwise impervious to probes designed using the previously established parameters. We show that the introduction of LNA nucleotides into 2′-O-methyl RNA oligonucleotides enables the design of shorter hairpin variants that match the probe−target stabilities of longer 2′-O-methyl RNA probes.

We demonstrate that these "tiny molecular beacons" are stable, bright, highly specific, and effective in binding mRNA target sites in live *D. melanogaster* oocytes. In *D. melanogaster* egg chambers, mRNAs are transcribed in the nurse cell nuclei throughout oogenesis and are transported into the oocyte *via* connecting ring canals. *oskar* mRNA localizes during midoogenesis at the posterior pole of the oocyte, while briefly anchoring at the anterior cortex in the earlier stages[25] (Figure 1, panel c). We have previously used 2′-O-methyl RNA molecular beacons to directly visualize the endogenous expression of *oskar* mRNA in *D. melanogaster* oocytes.[26] Following our report,

others have confirmed the target specificity of molecular beacons within various cellular contexts.[11−13] Here, we explored the *in vivo* accessibility of previously selected *oskar* mRNA target regions, utilizing tiny molecular beacons.

We found that tiny molecular beacons have better access than conventional molecular beacons to previously less accessible target sites. When designed as shorter hairpins for the same target region, they hybridized to the target region faster than their classical counterparts. By incorporating just three LNA nucleotides, well spaced by two 2′-*O*-methylribonucleotides, a tiny molecular beacon outperformed the same size probe that contained only a 2′-*O*-methylribonucleotide backbone, and the chimera tiny molecular beacon generated a fluorescence signal that was four times brighter.

The implementation of these changes in molecular beacon design will enable the targeting of highly structured mRNAs and the simultaneous visualization of several different mRNAs in live cells.

■ RESULTS AND DISCUSSION

Access to Target Sites. Theoretically, any sequence within a target RNA can be chosen as a site for a probe to bind. However, the extent of target accessibility is primarily a consequence of complex secondary and tertiary intramolecular foldings, which are difficult to closely predict.[24] In order to compare the accessibility of various target regions in a structured RNA, we chose *oskar* mRNA, which is expressed in *D. melanogaster* during oogenesis. We have previously designed molecular beacons that target several regions within this 3kB transcript[14] (Supplemental Figure S1). For this study, we focused on two regions, 1214−1238 and 2209−2233, the numbers representing the nucleotide position in *oskar* mRNA, in the 5′ to 3′ direction. According to the literature to date, there is no evidence that these regions are involved in mRNA−protein interactions. Both regions are slightly structured with some single-stranded stretches, but molecular beacons (Figure 2, panel a) designed to target these regions exhibit a different outcome when hybridized to the target RNA, when tested both *in vitro* and *in vivo*. When each probe is hybridized to *in vitro* transcribed *oskar* RNA under plausible physiological conditions at 25 °C, only the *2′OMe-RNA 2209* molecular beacon, targeting the 2209−2233 region, binds efficiently to the full-length transcript (Figure 2, panel b), and the same is observed *in vivo* (Figure 2, panel c, Supplemental Videos S1 and S10). The absolute fluorescence intensity of the signal generated 20 min post-microinjection was measured across a region of the oocyte that encompassed the posterior pole (Figure 2, panel d). The fluorescence intensity scale was plotted to 20,000 units such that all other intensity graphs could be compared among each other. To demonstrate the specificity of these probes, we performed hybridization reactions with antisense *oskar* RNA. With both molecular beacons, the fluorescence signal remained within background levels (data not shown).

When these molecular beacons were redesigned so that they contained shorter hairpins (11 nucleotide loops, 4 base pair stems) and a few 2′-*O*-methylribonucleotides were substituted with LNA nucleotides within the hairpin loop (Figure 3, panel a), both probes easily accessed their targets sites (Figure 3, panels b and c, Supplemental Videos S2−S5). The shorter hairpin loop allowed for easier access to the target region, and the presence of the LNA nucleotides increased the stability of the shorter probe−target hybrids. When compared to the signal intensity generated by *2′OMe-RNA* probes, *LNA/2′OMe-RNA*
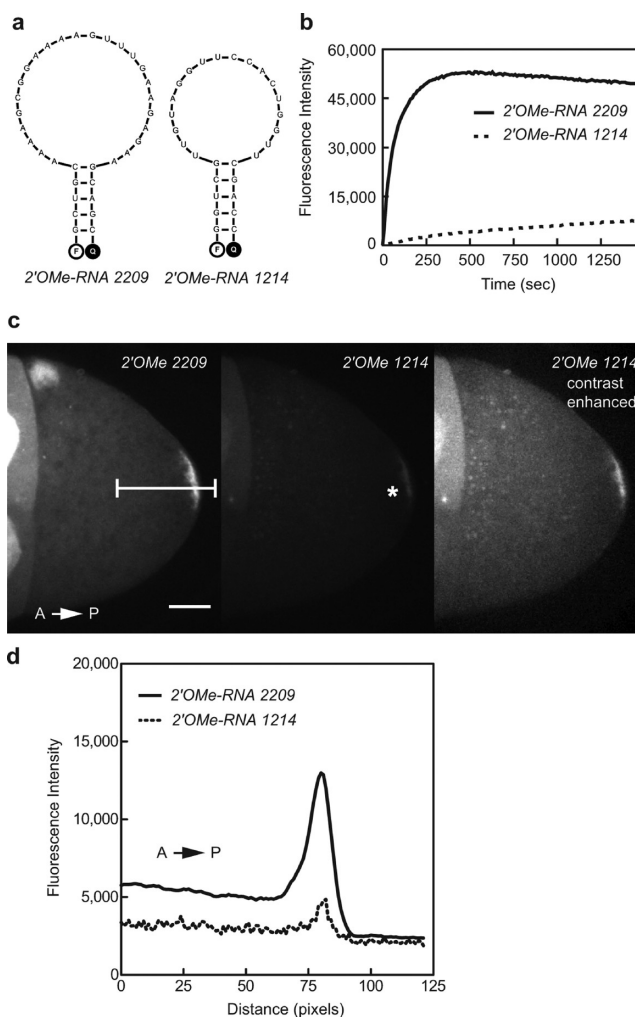

Figure 2. Conventional molecular beacons: design and characterization. (a) Predicted structures for two conventional molecular beacons that specifically target *oskar* mRNA. They are named on the basis of the first nucleotide position within the *oskar* transcript of the region that they target. (b) Hybridization profile for each probe with *in vitro* transcribed *oskar* mRNA. Time zero indicates the addition of the RNA to the molecular beacon solution. The *2′OMe-RNA 2209*-Cy5 probe showed better accessibility to the target compared to that of the *2′OMe-RNA 1214*-TMR probe. (c) The *in vitro* results were coordinated with the *in vivo* results obtained by imaging *oskar* mRNA localization using each probe. When a solution containing the same concentration of each probe was microinjected into live egg chambers, the *2′OMe-RNA 2209* probe gave a robust signal, whereas the *2′OMe-RNA 1214* probe resulted in a very faint signal (*) (Supplemental Video S1). Images represent projections of five 1 μm Z-sections at the 20 min time-point. Posterior is to the right. Scale bar is 20 μm. (d) Quantification of *oskar* mRNA localization in the oocyte in panel c. The absolute fluorescence intensity measured for each probe along a region (10 μm wide), depicted by the line in the first panel, beginning in the center of the oocyte cytoplasm and extending through and past the oocyte's posterior. Posterior maxima are aligned.

molecular beacons illuminate more than twice as brightly (Figure 3, panels b and d).

For region 1214−1238, we designed a tiny molecular beacon in which we substituted LNA nucleotides for two guanosines and three adenosines of 2′-*O*-methylribonucleotides (*LNA/2′OMe-RNA 1227*). We compared the fluorescence signal generated upon target[16] binding by this tiny molecular beacon with the conventional molecular beacon *2′OMe-RNA 1214*. In
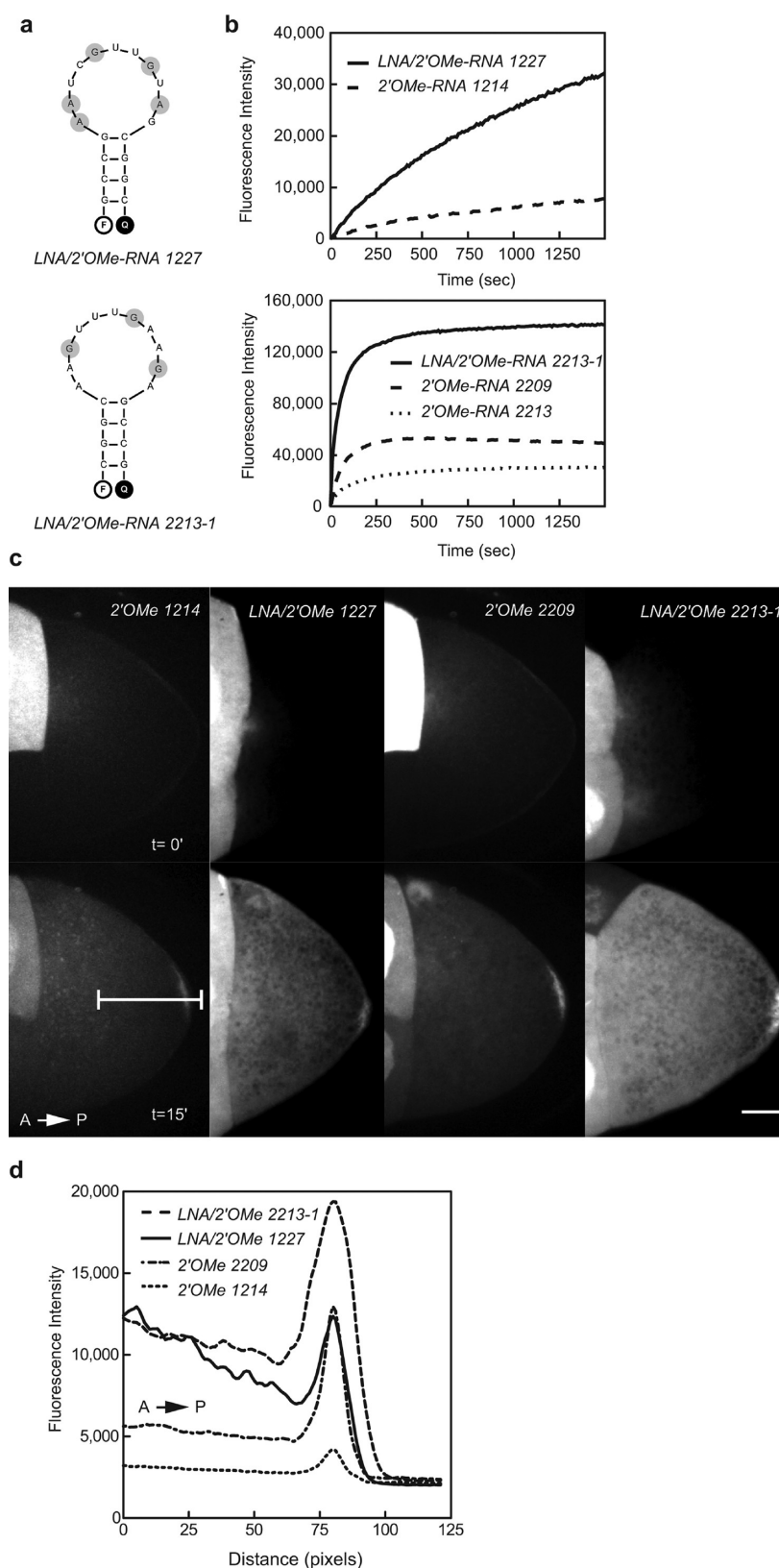
Figure 3. Tiny molecular beacons: design and characterization. (a) Predicted structures for two tiny molecular beacons targeting the same *oskar* mRNA regions as the conventional molecular beacons presented in Figure 2. LNA nucleotides are highlighted in gray. (b) Hybridization profiles for tiny molecular beacons with *in vitro* transcribed *oskar* RNA. Corresponding conventional probes were compared with tiny molecular beacons. LNA substitutions lead to an improved hybridization signal when compared to conventional molecular beacons (*2′OMe-RNA 1214*, *2′OMe-RNA 2209*, *2′OMe-RNA 2213*), as observed for the *LNA/2′OMe-RNA 1227* and *LNA/2′OMe-RNA 2213-1* probes. Time zero indicates the addition of the RNA to the molecular beacon solution. (c) *In vivo* imaging profiles of molecular beacons with endogenous *oskar* mRNA corresponding to the *in vitro* data. When microinjected into live egg chambers, the *LNA/2′OMe-RNA 1227* probe and the *LNA/2′OMe-RNA 2213-1* probe gave a brighter signal

Figure 3. continued

compared to the signals obtained with corresponding conventional probes (*2′OMe-RNA 1214* and *2′OMe-RNA 2209*) (Supplemental Videos S2–S5). Top panels represent time zero, the beginning of time-lapse acquisition, which is within a few seconds from microinjection of the probe into a nurse cell most proximal to the oocyte. Images are projections of five 1 μm Z-sections. Bottom panels represent the corresponding Z-projections after 15 min. Posterior is to the right. Scale bar is 20 μm. (d) Quantification of *oskar* mRNA localization in the oocytes from bottom panels in panel c. The absolute fluorescence intensity measured for each probe along a region (10 μm wide), depicted by the line in the first panel, beginning in the center of the oocyte cytoplasm and extending through and past the oocyte's posterior. For each oocyte, the orientation of the line depended on the distribution of the signal at the posterior pole. Posterior maxima are aligned.

Table 1. Molecular Beacon Sequences and Their Labels[a]

name	sequence (5′–3′)
2′OMe-RNA 1214	TMR – *ggucg* UUGUAGGUUCCACUGGUU *cgacc* – BHQ-2
2′OMe-RNA 2209	Cy5 – *gcugc* AAAAGCGGAAAAGUUUGAAGAGAA *gcagc* – BHQ-2
2′OMe-RNA 2213	TMR – *cggc* AAGUUUGAAGA *Gccg* – dabcyl
LNA/2′OMe-RNA 1227	TMR – *gccG* A<u>A</u>UC<u>G</u>UU<u>G</u>U<u>A</u>G *cggc* – dabcyl
LNA/2′OMe-RNA 2210-1	TMR – *gcc* <u>G</u>A<u>A</u>GA<u>G</u>AA *Ggc* – dabcyl
LNA/2′OMe-RNA 2210-2	TMR – *gcc* <u>GAAGAGAA</u> *Ggc* – dabcyl
LNA/2′OMe-RNA 2213-1	TMR – *cggc* AA<u>G</u>UUU<u>G</u>AA<u>G</u>A *Gccg* – dabcyl
LNA/2′OMe-RNA 2213-2	TMR – *cggc* A<u>AG</u>UUU<u>G</u>AA<u>G</u>A *Gccg* – dabcyl

[a]<u>underlined nucleotides</u> = LNA; *italic nucleotides* = stem sequence; UPPER CASE nucleotides = probe sequence; TMR = tetramethylrhodamine; BHQ-2 = Black Hole Quencher 2.

in vitro experiments, the signal intensity increased more than 4-fold with the tiny molecular beacon, indicating increased accessibility to that target region (Figure 3, panel b). When the probes were microinjected into live egg chambers, the signal generated by the tiny *LNA/2′OMe-RNA 1227* molecular beacon was far superior to the signal observed with the conventional *2′OMe-RNA 1214* (Figure 3, panel c, Supplemental Videos S1, S2, and S4).

To determine whether the enhanced performance was due to the reduced size of the molecular beacon hairpin or due to a combination effect of the size and the presence of LNA nucleotides, we compared 2′-*O*-methyl RNA and LNA/2′-*O*-methyl RNA chimera tiny molecular beacons with conventional 2′-*O*-methyl RNA molecular beacons (Figure 3, panel b). For region 2209–2233, we designed a tiny molecular beacon containing only 2′-*O*-methylribonucleotides (*2′OMe-RNA 2213*). The fluorescence intensity generated when the *2′OMe-RNA 2213* probe hybridized to the RNA *in vitro* was 1.8 times lower than the fluorescence intensity obtained with the conventional *2′OMe-RNA 2209* molecular beacon (Figure 3, panel b). Yet, when we substituted three LNA guanosines for three 2′-*O*-methylribonucleotides in the loop region (*LNA/2′OMe-RNA 2213-1*), the signal increased by more than 4.7 times, as compared to the intensity of the signal obtained with the 2′-*O*-methyl RNA tiny molecular beacon. We performed microinjections in *D. melanogaster* oocytes, at stages when *oskar* mRNA becomes localized at the posterior region of the oocyte. The tiny molecular beacons diffused quickly into the oocyte's cytoplasm and hybridized to the localized *oskar* mRNA at the posterior end. The fluorescence signal observed after micro-injection into live egg chambers of each probe mirrored the *in vitro* RNA hybridization results with the tiny molecular beacons binding to the RNA target at faster rates. This is particularly visible in dual injections where the conventional *2′OMe-RNA 2209* molecular beacon failed to yield a posterior signal when it competed against the *LNA/2′OMe-RNA 2213-1* tiny molecular beacon for the same target region (Supplemental Videos S3 and S5). The ratio of *in vivo* fluorescence signals at the posterior for *LNA/2′OMe-RNA vs 2′OMe-RNA* molecular beacons indicate a

1.5-fold and 3-fold increase for 2209 and 1214 target regions, respectively. The absolute fluorescence intensity measurements reveal a higher fluorescence signal in the middle of the oocytes with *LNA/2′OMe-RNA* probes than with conventional probes (Figure 3, panel c). There are several explanations that could account for the increase in signal: (1) tiny molecular beacons bind faster and more readily to target RNA, therefore detecting molecules that are not yet localized at the posterior; (2) tiny molecular beacons are labeled with dabcyl quencher, whereas the conventional molecular beacons are labeled with Black Hole Quencher, a moiety known to increase the stability of the stem structure that therefore retards the hybridization rate of the probe to the target site (Table 1); or (3) tiny molecular beacons are slightly less specific due to their shorter probe and stem regions.

Variations of the Number and Position of LNA Substitutions in the Hairpin Loop. Encouraged by our positive results for LNA substitutions, we analyzed several variations in the number and location where the LNA nucleotides were introduced into the hairpin loop of the tiny molecular beacons. We compared a probe containing three LNA guanosines separated from each other by at least two nucleotides (*LNA/2′OMe-RNA 2213-1*), to a probe containing three LNA adenosines and two LNA guanosines, some adjacent to each other and some separated by one nucleotide (*LNA/2′OMe-RNA 2213-2*) (Figure 4, panel a). The results showed that the maximum fluorescence intensity generated by the *LNA/2′OMe-RNA 2213-1* probe *in vitro* was 2-fold greater than the maximum fluorescence intensity of the *LNA/2′OMe-RNA 2213-2*, and fluorescence intensity of the *LNA/2′OMe-RNA 2213-1* probe was 4 times greater than the signal obtained with its 2′-*O*-methyl RNA backbone counterpart (*2′OMe-RNA 2213*) (Figures 4, panel b). When comparing a shorter hairpin loop design (eight nucleotides) possessing two LNA adenosines and two LNA guanosines in its loop (*LNA/2′OMe-RNA 2210-1*) to a probe of the same length containing five LNA adenosines and three LNA guanosines in its loop (*LNA/2′OMe-RNA 2210-2*) (Figure 4, panel c), we observed that increasing the number of LNA nucleotides and incorporating them next to each other
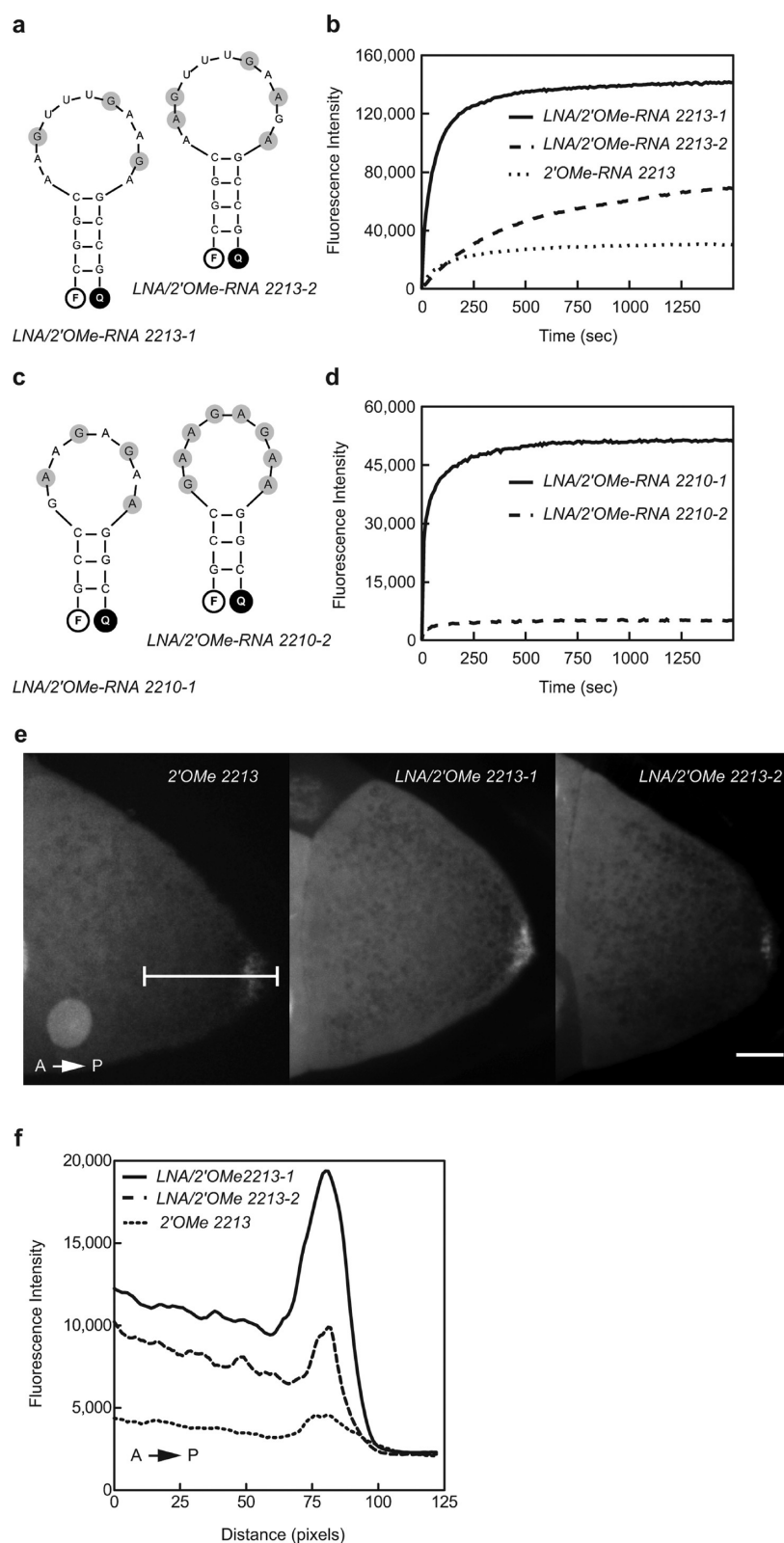
Figure 4. Only a few LNA substitutions are required for tiny molecular beacons to be efficient probes for detecting mRNA *in vitro* and *in vivo*. (a) *LNA/2'OMe-RNA 2213* probes with three or five LNA substitutions (highlighted in gray). (b) *In vitro* RNA hybridization studies of molecular beacons with *in vitro* transcribed target RNA. The LNA substitutions (*LNA/2'OMe-RNA 2213-1* and *LNA/2'OMe-RNA 2213-2*) improved tiny molecular beacon performance when compared to the corresponding 2'-O-Me-RNA molecular beacon (*2'OMe-RNA 2213*). However, the tiny molecular beacon's capability to efficiently hybridize with target RNA was reduced when the number of LNA nucleotides was increased from three to five (*LNA/2'OMe-RNA 2213-2*). (c) *LNA/2'OMe-RNA 2210* probes with four or eight LNA substitutions (highlighted in gray). (d) *In vitro* RNA-hybridization studies of molecular beacons with *in vitro* transcribed target RNA. The length of the probes was shortened from 11 (probes in panel a) to 8 nucleotides, and LNA substitutions were increased from 3 and 5 to 4 and 8. The tiny molecular beacon was able to hybridize to its target when four LNA nucleotides were present. When the number of LNA nucleotides was increased to eight, the tiny molecular beacon's performance dropped

Figure 4. continued

dramatically. Increasing the number of LNA nucleotides did not translate into better target detection *in vitro*. This was also observed *in vivo*, where probe *LNA/2'OMe-RNA 2210-2* failed to detect endogenous *oskar* mRNA (Supplemental Video S9). (e) *In vivo*, both LNA/2'-O-Me-RNA chimera tiny molecular beacons (*LNA/2'OMe-RNA 2213-1* and *LNA/2'OMe-RNA 2213-2*) showed better target detection when compared to the *2'OMe-RNA 2213* variant (Supplemental Videos S6−S8). Images represent projections of five 1 μm Z-sections at the 15 min time-point. Posterior is to the right. Scale bar is 20 μm. (f) Quantification of *oskar* mRNA localization in the oocytes in panel e. The absolute fluorescence intensity measured for each probe along a region (10 μm wide), depicted by an example line in the first panel, beginning in the center of the oocyte cytoplasm and extending through and past the oocyte's posterior. Posterior maxima are aligned.

inhibited the rate of hybridization and decreased the probe's accessibility to the target site (Figure 4, panel d). The *in vitro* fluorescence signal was 6 times higher when the probe contained just three LNA nucleotides, compared to using the probe that contained LNA nucleotides in all eight positions in the loop. However, both probes showed a weaker *in vitro* fluorescence signal than when using the conventional molecular beacon, *2'OMe-RNA 2209*. When microinjected into live egg chambers, the *LNA/2'OMe-RNA 2213-1* probe generated the brightest signal at the posterior among all other probes (Figure 4, panels e and f and Supplemental Videos S6−8), whereas *LNA/2'OMe-RNA 2210-2* failed to detect *oskar* mRNA (Supplemental Video S9).

Variations of Loop and Stem Length. The hairpin structure of molecular beacons gives these probes the characteristic of being extremely specific, discriminating against even just one single nucleotide mismatch.[20,27] This property makes them ideal for the detection of short stretches of RNA that may vary very little among hundreds of RNA species. Tiny molecular beacons are shorter hairpin probes that are half the size of the classical molecular beacons, with loops ranging in length between 8 to 11 nucleotides and stems of 3 to 4 nucleotides.

We explored two designs for tiny molecular beacons, one having a loop of 8 nucleotides and a stem of 3 base pairs (*LNA/2'OMe-RNA 2210-1*), and the other having a loop of 11 nucleotides and a stem of 4 base pairs (*LNA/2'OMe-RNA 2213-1*) (Figure 5, panel a). They both accessed the target site at the same rate, yet the strongest signal was observed with the longer probe (*LNA/2'OMe-RNA 2213-1*) (Figure 5, panel b). However, when the probe−target hybrids were denatured as the temperature increased from 25 to 90 °C, the shorter probe (*LNA/2'OMe-RNA 2210-1*) indicated better stability on target RNA, as reflected by a higher melting temperature (T_m) (Figure 5, panel c). The thermal profiles revealed that tiny molecular beacons containing LNA nucleotides were more stable than their 2'-O-methyl RNA counterpart. *LNA/2'OMe-RNA 2213-1* and *LNA/2'OMe-RNA 2210-1* had 13 and 17 °C higher T_m, respectively. Also, decreasing the probe−target hybrid length, but incorporating additional LNA nucleotides enhanced the stability of the shorter hybrid, as seen by the rise in T_m from 58 to 62 °C (*LNA/2'OMe-RNA 2213-1* vs *LNA/2'OMe-RNA 2210-1*).

Conclusion. Molecular beacons previously designed for *in vivo* imaging and synthesized from 2'-O-methylribonucletides are normally designed to have five to six base pair stems (with a low GC content) and 15 to 30 nucleotides in the probe (loop) region of the hairpin structure, which ensures that there is more than a 10 °C difference between the melting temperature of the probe−target hybrid and the temperature at which the target is detected *in vivo* at 25 or 37 °C.

With the incorporation of LNA nucleotides into the loop of the hairpin, the stability of the probe−target hybrid increases,
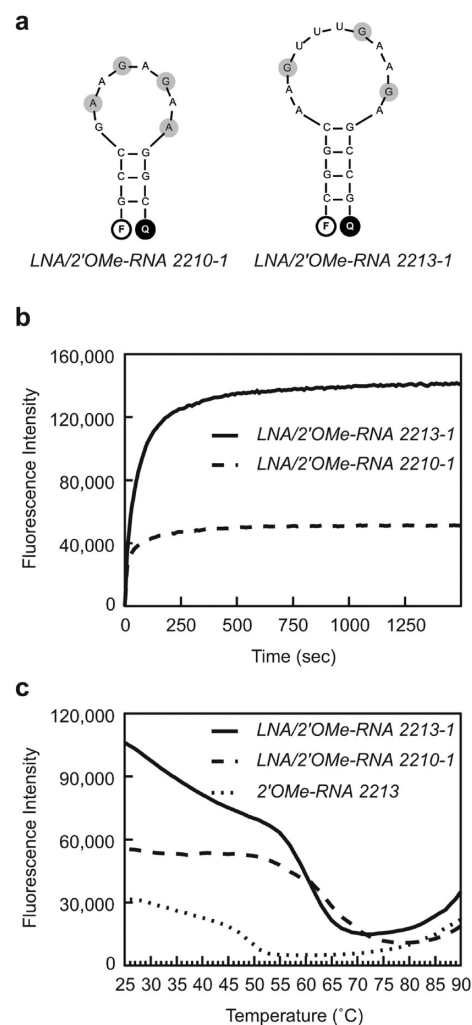

Figure 5. Effect of loop/stem variations on tiny molecular beacon hybridization efficiency. (a) Design of two LNA/2'-O-Me-RNA tiny molecular beacons targeting the same region of *oskar* mRNA (*LNA/2'OMe-RNA 2213-1* vs *LNA/2'OMe-RNA 2210-1*). LNA nucleotides are highlighted in gray. These tiny molecular beacons have an 11-nucleotide loop and 4 base pair stem, and an 8-nucleotide loop and a 3 base pair stem, respectively. (b) When compared *in vitro*, the slightly longer LNA/2'-O-Me-RNA tiny molecular beacon (*LNA/2'OMe-RNA 2213-1*) outperformed the shorter probe (*LNA/2'OMe-RNA 2210-1*). (c) Probe-target hybrids obtained from the RNA hybridization experiments in panel b were heat denatured by slowly increasing the temperature. Their fluorescence intensity was recorded for every 2 °C increase. The T_m for LNA/2'-O-Me-RNA probes were 58 °C (*LNA/2'OMe-RNA 2213-1*) and 62 °C (*LNA/2'OMe-RNA 2210-1*), both higher than the T_m observed for the *2'OMe-RNA 2213* molecular beacon for which the T_m was only 45 °C.

enabling the design of probes with shorter hairpin loops and shorter stems. Tiny molecular beacons are chimeras with LNA/

2′-O-methyl RNA loops and 2′-O-methyl RNA stems. They consist of 3 to 4 base-pair-long stems (containing only GC pairs) and 8 to 11 nucleotide-long hairpin loops. We found that when designing the probe sequence, which is of course dependent on the target sequence, it is best to avoid stretches of 3 or more guanosines or cytosines, to keep the loop GC-content between 30 to 60%, and it is best to avoid including only LNA nucleotides.

Here, we compared the accessibility of tiny molecular beacons to two regions of *oskar* mRNA for which we previously designed and characterized conventional molecular beacons. We found that tiny molecular beacons have better access than conventional molecular beacons to previously less accessible target sites, as was observed for region 1214−1238 of *oskar* mRNA. In addition, since the new probes were designed as shorter hairpins for the same target region, with comparable target-binding energy when LNA nucleotides were incorporated, they annealed to the target faster than their classical counterparts, making them better fit probes for "finding" the target sequence within the structure of the RNA. By incorporating just three LNA nucleotides, well spaced by two 2′-O-methylribonucleotides, a tiny molecular beacon outperformed the same size probe composed of only a 2′-O-methyl RNA backbone. Denaturation profiles show that the latter did not stay hybridized to its target as stably as the LNA-containing counterpart, having the equilibrium shifted toward the hairpin conformation rather than the open/annealed-to-target conformation. However, a tiny molecular beacon synthesized from all LNA nucleotides in the hairpin loop region performed even worse in the hybridization reaction with the target RNA. This may be due to the steric hindrance placed by the carbon bridge of the LNA on the formation of the hybrid double helix.[23]

When different sizes of tiny molecular beacons were compared, we found that a hairpin containing an 8 nucleotide loop and a 3 base pair stem did not fair as well as a hairpin consisting of an 11 nucleotide loop and a 4 base pair stem, in which respective 9 base pair hybrids and 12 base pair hybrids were formed with the RNA target. Conversely, the shorter hairpin possessing four LNA nucleotides formed a stronger probe−target hybrid than the longer hairpin possessing three LNA nucleotides, yet it yielded a less intense signal. It is possible that the emission of the fluorophore is quenched across the short length of the probe−target hybrid, resulting in a lower signal. This result indicates that a balance between probe length and LNA substitutions can yield an optimal probe for *in vivo* detections of mRNAs.

We have previously tracked *oskar* mRNA in live oocytes using a cocktail of four classical molecular beacons. We analyzed its movement into different compartments of the egg chamber over time using a custom 4D tracking algorithm (QUAI).[15] Our studies have aided in refining the model for *oskar* transport posited by a contemporaneous study by Zimyanin *et al.* using *oskar*-MS2-GFP.[28] In this study, *oskar* mRNA is tagged with 10 copies of a hairpin sequence that acts as target for the bacteriophage coat protein MS2 fused to green fluorescent protein (GFP), thus identifying the transcript.

We tested the sensitivity of the tiny molecular beacons, by microinjecting a cocktail of two tiny molecular beacons (*LNA/2′OMe-RNA 2213-1* and *LNA/2′OMe-RNA 1227* labeled with TMR) in egg chambers expressing the *oskar*-MS2-GFP system (Supplemental Video S11). The colocalization pattern of the TMR and GFP signals indicates that the tiny molecular beacons

do not preferentially diffuse to the posterior of the oocyte, but bind to *oskar* mRNA while it is being transported (Supplemental Video S12). Moreover, we tracked the movement of *oskar* mRNPs during various stages of oogenesis (Supplemental Videos S13 and S14). Our results indicate that tiny molecular beacons are indeed able to visualize an endogenous RNA target as it is being transported over time. We are now optimizing the imaging conditions to enable an increased sensitive detection of the wide size range of mRNA particles. Designing several tiny molecular beacons to target different RNA regions of the same mRNA will increase the signal per target molecule, thereby enabling the visualization of low abundance RNAs.

Lastly, the application of tiny molecular beacons can be extended to detection of small noncoding RNAs, such as microRNAs or piRNAs in living cells, which are only 21−27 nucleotides long.[29]

■ METHODS

Design and Synthesis of Tiny Molecular Beacons. For our study, we used one of the most complete algorithms using nearest neighbor thermodynamic rules: Zuker's *mfold* package.[16] Using Zuker's open access web server, http://mfold.rna.albany.edu/?q=mfold, we folded all the molecular beacon sequences. Though the parameters carrying weight in the prediction output, such as salt concentrations and temperature, are fixed at nonphysiological conditions, we obtained an optimal fold and a range of suboptimal folds for each probe, which were all carefully considered when designing the hairpin. This allowed us to compare the structures and free energy of each optimal and suboptimal structure for each probe, as well as to compare different probes under the same conditions.

The design and synthesis of tiny LNA/2′-O-methyl RNA chimera molecular beacons, as well as a refined approach for the selection of target regions, are described in our previous publication that appeared in the *Methods and Protocols* chapter of the Methods in Molecular Biology Series.[30] LNA/2′-O-methyl RNA oligonucleotides were synthesized using standard automatic DNA/RNA synthesis chemistries,[31] except that the phosphoramidite coupling and oxidation steps in each synthesis cycle were doubled. LNA phosphoramidites were acquired from Exiqon and 2′-O-methyl RNA phosphoramidites from Glen Research; dabcyl and black hole quencher 2 (BHQ-2) CPG columns were purchased from Biosearch Technologies, and tetramethylrhodamine (TMR) fluorophore from Invitrogen and Cy5 fluorophore from GE Healthcare Life Sciences. Additional detailed protocols for the synthesis and characterization of tiny molecular beacons are available at http://www.molecular-beacons.org/. Sequences and labels of the molecular beacons used in this study are listed in Table 1.

In Vitro **Hybridization and Thermal Denaturation Profiles with RNA.** *oskar* mRNA sense strand was *in vitro* transcribed according to the manufacturer's instructions using a T7MegaScript Ambion Kit (Life Technologies-Ambion) using a PCR fragment amplified from a plasmid containing *oskar* cDNA inserted into a pBluescript KS+ vector (kind gift from R. Lehmann, NYU Medical School). *oskar* mRNA antisense strand was *in vitro* transcribed using the same kit from the same plasmid, which was first linearized by digestion with Hind III restriction endonuclease (New England Biolabs).

Ten microliter aliquots of 600 nM RNA in 50 mM Tris-HCl (pH 7.5), 1.5 mM MgCl$_2$ and 100 mM NaCl (hybridization buffer) were unfolded at 90 °C degrees for 10 s and immediately placed on ice. The RNA solution was allowed to reach RT before probe-RNA hybridization analysis.

Hybridization reactions were performed at 25 °C, in a 60 μL total volume containing 80 nM molecular beacon and 100 nM *oskar* mRNA sense strand or antisense strand in hybridization buffer. The change in fluorescence intensity was measured using a Fluoromax-4 photon-counting spectrofluorometer (Horiba-Jobin Yvon). The fluorescence

signal was monitored, first with just the hybridization buffer, then with the molecular beacon, and last with addition of the RNA target. It was recorded every 10 s, with an integration occurring over 2 s. The excitation and emission slit widths were 3 and 2 nm, respectively, with excitation/emission wavelengths of 555/580 nm and 649/670 nm for TMR and Cy5, respectively.

Thermal denaturation reactions were performed in the same spectrofluorometer, using a Peltier cooler and temperature controller (Horiba-Jobin Yvon). Each probe−target solution was heated from 25 to 90 °C, and the fluorescence intensity was recorded for every 2 °C increase after 30 s equilibration.

The hybridization and thermal denaturing curves are representative of two or more individual experiments.

Microinjection and *in Vivo* Imaging. Newly hatched Oregon R or *oskar*-MS2-GFP-expressing female flies (kind gift from D. St Johnston) female flies were fed fresh yeast paste for 2−4 days. Ovaries were dissected in Halocarbon Oil 700 (Sigma-Aldrich) directly on a glass coverslip and then teased apart into individual egg chambers. After mounting the glass coverslip onto the stage of the spinning disk microscope, 200 ng μL^{-1} (~30 μM) molecular beacon solution (2′-O-methyl RNA and/or LNA/2′-O-methyl RNA chimera) in hybridization buffer was microinjected into the nurse cell most proximal to the oocyte. The selected egg chambers were at stages 8 or older.

Imaging commenced within seconds after microinjection on a Leica DMI-4000B inverted microscope (Leica Microsystems Inc.) mounted on a TMC isolation platform (Technical Manufacturing Corporation), with a Yokogawa CSU 10 spinning disk head and Hamamatsu C9100-13 ImagEM EMCCD camera (Perkin-Elmer). The microscopy set up includes diode lasers (491, 561, and 638 nm (Spectra Services Inc.)) and an Eppendorf Patchman-Femtojet microinjector (Eppendorf Inc.). The images were acquired with a 40X/1.25−0.75 oil objective, using Volocity 5.3.3 acquisition software (Perkin-Elmer) and then processed with ImageJ software (NIH).[32] Images are representative of three or more individual injections, and are a projection of five Z-sections (1 μm each).

For tracking endogenous *oskar* mRNA particles throughout the oocyte with tiny molecular beacons, we acquired images using a 63X/1.40−0.60 oil objective. Acquisition was initiated 15−25 min after microinjection, for up to 21 Z-slices of 0.25−0.5 μm thickness, imaging every 30 s (Oregon R egg chambers) or 2 min (*oskar*-MS2-GFP) for the duration of up to 30 min. The colocalization of signals generated by tiny molecular beacons and *oskar*-MS2-GFP system was determined after 20 min from oocyte microinjection.

Particle Tracking. We used Imaris 7.4.2 (Bitplane Scientific Software) to track particles as "spots". The estimated spot diameter was 2.4 μm, and the allowed maximum travel distance for each spot was 3 μm. Using the same parameters, we also tracked particles observed in the oocyte that was microinjected with classical molecular beacons (Supplementary Video S1). Acquisition for dual micro-injections with probes labeled with distinct fluorophores was performed first in the Z direction and then for each channel, collecting five Z-slices (1 μm) with 700 ms exposure every minute for 30 min. This acquisition protocol leads to a displacement for red or green spots that represent particles with both probes bound to the same mRNP.

ASSOCIATED CONTENT

Ⓢ Supporting Information

This material is available free of charge *via* the Internet at http://pubs.acs.org.

AUTHOR INFORMATION

Corresponding Author

*E-mail: bratu@genectr.hunter.cuny.edu.

Notes

The authors declare no competing financial interest.

REFERENCES

(1) Tautz, D., and Pfeifle, C. (1989) A non-radioactive in situ hybridization method for the localization of specific RNAs in Drosophila embryos reveals translational control of the segmentation gene hunchback. *Chromosoma 98*, 81−85.

(2) Ainger, K., Avossa, D., Morgan, F., Hill, S. J., Barry, C., Barbarese, E., and Carson, J. H. (1993) Transport and localization of exogenous myelin basic protein mRNA microinjected into oligodendrocytes. *J. Cell Biol. 123*, 431−441.

(3) Cha, B. J., Koppetsch, B. S., and Theurkauf, W. E. (2001) In vivo analysis of Drosophila bicoid mRNA localization reveals a novel microtubule-dependent axis specification pathway. *Cell 106*, 35−46.

(4) Glotzer, J. B., Saffrich, R., Glotzer, M., and Ephrussi, A. (1997) Cytoplasmic flows localize injected oskar RNA in Drosophila oocytes. *Curr. Biol. 7*, 326−337.

(5) MacDougall, N., Clark, A., MacDougall, E., and Davis, I. (2003) Drosophila gurken (TGFalpha) mRNA localizes as particles that move within the oocyte in two dynein-dependent steps. *Dev. Cell. 4*, 307−319.

(6) Hachet, O., and Ephrussi, A. (2004) Splicing of oskar RNA in the nucleus is coupled to its cytoplasmic localization. *Nature 428*, 959−963.

(7) Fusco, D., Accornero, N., Lavoie, B., Shenoy, S. M., Blanchard, J. M., Singer, R. H., and Bertrand, E. (2003) Single mRNA molecules demonstrate probabilistic movement in living mammalian cells. *Curr. Biol. 13*, 161−167.

(8) Forrest, K. M., and Gavis, E. R. (2003) Live imaging of endogenous RNA reveals a diffusion and entrapment mechanism for nanos mRNA localization in Drosophila. *Curr. Biol. 13*, 1159−1168.

(9) Tyagi, S. (2009) Imaging intracellular RNA distribution and dynamics in living cells. *Nat. Methods 6*, 331−338.

(10) Tyagi, S., and Kramer, F. R. (1996) Molecular beacons: probes that fluoresce upon hybridization. *Nat. Biotechnol. 14*, 303−308.

(11) Kloc, M., Wilk, K., Vargas, D., Shirato, Y., Bilinski, S., and Etkin, L. D. (2005) Potential structural role of non-coding and coding RNAs in the organization of the cytoskeleton at the vegetal cortex of Xenopus oocytes. *Development 132*, 3445−3457.

(12) Vargas, D. Y., Raj, A., Marras, S. A., Kramer, F. R., and Tyagi, S. (2005) Mechanism of mRNA transport in the nucleus. *Proc. Natl. Acad. Sci. U.S.A. 102*, 17008−17013.

(13) Tyagi, S., and Alsmadi, O. (2004) Imaging native beta-actin mRNA in motile fibroblasts. *Biophys. J. 87*, 4153−4162.

(14) Bratu, D. P. (2003) Imaging native mRNAs in living Drosophila oocytes using molecular beacons, in *UMI Dissertation Services, #3105839*, Doctoral Thesis, New York University, New York.

(15) Mhlanga, M. M., Bratu, D. P., Genovesio, A., Rybarska, A., Chenouard, N., Nehrbass, U., and Olivo-Marin, J. C. (2009) In vivo colocalisation of oskar mRNA and trans-acting proteins revealed by quantitative imaging of the Drosophila oocyte. *PLoS One 4*, e6241.

(16) Zuker, M. (2003) Mfold web server for nucleic acid folding and hybridization prediction. *Nucleic Acids Res. 31*, 3406−3415.

(17) Mathews, D. H., Sabina, J., Zuker, M., and Turner, D. H. (1999) Expanded sequence dependence of thermodynamic parameters improves prediction of RNA secondary structure. *J. Mol. Biol. 288*, 911−940.

(18) Molenaar, C., Marras, S. A., Slats, J. C., Truffert, J. C., Lemaitre, M., Raap, A. K., Dirks, R. W., and Tanke, H. J. (2001) Linear 2′-O-methyl RNA probes for the visualization of RNA in living cells. *Nucleic Acids Res. 29*, e89.

(19) Wang, L., Yang, C. J., Medley, C. D., Benner, S. A., and Tan, W. (2005) Locked nucleic acid molecular beacons. *J. Am. Chem. Soc. 127*, 15664−15665.

(20) Tyagi, S., Bratu, D. P., and Kramer, F. R. (1998) Multicolor molecular beacons for allele discrimination. *Nat. Biotechnol. 16*, 49−53.

(21) Bratu, D. P. (2006) Molecular beacons: Fluorescent probes for detection of endogenous mRNAs in living cells. *Methods Mol. Biol. 319*, 1−14.

(22) Koshkin, A. A., Fensholdt, J., Pfundheller, H. M., and Lomholt, C. (2001) A simplified and efficient route to 2′-O, 4′-C-methylene-linked bicyclic ribonucleosides (locked nucleic acid). *J. Org. Chem. 66*, 8504−8512.

(23) Kierzek, E., Ciesielska, A., Pasternak, K., Mathews, D. H., Turner, D. H., and Kierzek, R. (2005) The influence of locked nucleic acid residues on the thermodynamic properties of 2′-O-methyl RNA/RNA heteroduplexes. *Nucleic Acids Res. 33*, 5082−5093.

(24) Mathews, D. H., Turner, D. H., and Zuker, M. (2007) RNA secondary structure prediction. *Curr. Protoc. Nucleic Acid Chem. 28*, 11.2.1−11.2.17.

(25) St Johnston, D. (2005) Moving messages: The intracellular localization of mRNAs. *Nat. Rev. Mol. Cell. Biol. 6*, 363−375.

(26) Bratu, D. P., Cha, B. J., Mhlanga, M. M., Kramer, F. R., and Tyagi, S. (2003) Visualizing the distribution and transport of mRNAs in living cells. *Proc. Natl. Acad. Sci. U.S.A. 100*, 13308−13313.

(27) Bonnet, G., Tyagi, S., Libchaber, A., and Kramer, F. R. (1999) Thermodynamic basis of the enhanced specificity of structured DNA probes. *Proc. Natl. Acad. Sci. U.S.A. 96*, 6171−6176.

(28) Zimyanin, V. L., Belaya, K., Pecreaux, J., Gilchrist, M. J., Clark, A., Davis, I., and St Johnston, D. (2008) In vivo imaging of oskar mRNA transport reveals the mechanism of posterior localization. *Cell 134*, 843−853.

(29) Farazi, T. A., Juranek, S. A., and Tuschl, T. (2008) The growing catalog of small RNAs and their association with distinct Argonaute/Piwi family members. *Development 135*, 1201−1214.

(30) Bratu, D. P., Catrina, I. E., and Marras, S. A. (2011) Tiny molecular beacons for in vivo mRNA detection. *Methods Mol. Biol. 714*, 141−157.

(31) Mullah, B., and Livak, K. (1999) Efficient automated synthesis of molecular beacons. *Nucleosides, Nucleotides Nucleic Acids 18*, 1311−1312.

(32) Rasband, W. S. (1997−2011) *ImageJ*, U.S. National Institute of Health, Bethesda, MD, USA, http://imagej.nih.gov/ij/.